International Journal of Heat and Fluid Flow 118 (2026) 110177

Contents lists available at ScienceDirect

International Journal of Heat and Fluid Flow

journal homepage: www.elsevier.com/locate/ijhff

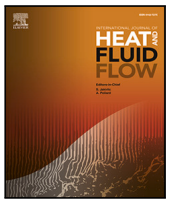

Experimental and numerical investigation of fast control surface deflections☆

Ruben B. Seidler [a,*], Reinhard Geisler [b], Andreas Schröder [b], Jochen Wild [a]

[a] Institute of Aerodynamics and Flow Technology, DLR, Lilienthalplatz 7, Braunschweig, 38102, Lower Saxony, Germany
[b] Institute of Aerodynamics and Flow Technology, DLR, Bunsenstraße 10, Göttingen, 37073, Lower Saxony, Germany

ARTICLE INFO

Keywords:
Load alleviation
Control surface
Unsteady aerodynamics
Wind tunnel experiment
Numerical simulation
Linear frequency domain

ABSTRACT

The development of load alleviation for an aircraft requires an accurate and efficient prediction of gust and maneuver loads. In the design of an aircraft the prediction of these unsteady loads has become crucial for the ideal alleviation of gust loads. A database for unsteady aerodynamic responses is however very cost expensive and time consuming to generate, in an experiment and with numerical simulations. An efficient tool for the computation of aerodynamic responses is the linear frequency domain solver, which allows the prediction of amplitude and phase shift of any periodic oscillation of body or flow in the frequency domain. The unsteady response allows a fast and efficient prediction for any arbitrary unsteady change of in example a control surface deflection or a gust speed. The validation of the linear frequency domain solver for unsteady aerodynamics is crucial, so that its prediction quality is ensured. A wind tunnel experiment was set up, which focused on fast control surface deflections and analyzed the capabilities and accuracy of the method. The experiment was accompanied by two- and three-dimensional URANS simulations, which allow a more detailed comparison and help to increase the understanding of the flow physics. For higher frequencies of the control surface oscillation, the adjusting position of the stagnation point on the leading edge lags behind the actual control surface position as if it were in a quasi-steady state. This leads to a phase lag between motion and resulting force and a lower lift response amplitude.

1. Introduction

In aviation there is a constant thrive to increase the efficiency and reduce the environmental impact of an aircraft. A promising technology for this objective is the implementation of load alleviation systems on an aircraft. Load alleviation thereby aims to reduce the aerodynamic forces and stresses on an aircraft structure, thus allowing to reduce the strength of required aircraft structures in its design. This leads to lighter aircraft structures, especially in the wing and reduces the overall weight of the aircraft, up to 4.4% of the operating empty mass (Handojo et al., 2022). In consequence, less lift is required to be generated by the wings and they can be designed smaller, which leads to less drag of the aircraft. Alternatively, the saved weight can be used to allow more passengers on the aircraft. In both cases, the fuel per passenger is reduced, which increases the efficiency of the aircraft and reduces its climate impact (Xu and Kroo, 2014). Active load alleviation describes a method, in where controllable systems, such as control surfaces, change the forces and moments and their distribution on the wing. For the alleviation of gust loads due to disturbances of the incoming flow, which can induce high forces on the structure, these systems need to react within real-time. In that case the impact of the unsteady aerodynamics become more important and needs to be known to the system, so that an ideal alleviation becomes possible (Giesseler et al., 2012). The implementation of a feed-forward system, which predicts the incoming loads before the incoming flow arrives at the wing, is beneficial to the potential of the load alleviation system, see Vuillemin et al. (2021) and Khalil and Fezans (2021). The time-resolved simulation of unsteady aerodynamics is currently still very expensive and time consuming, and it is necessary to use unsteady Reynolds-averaged Navier–Stokes equations (URANS) or other equally capable methods for an accurate prediction (Ghoreyshi et al., 2013). An alternative tool for the efficient simulation of unsteady aerodynamics is the linear frequency domain (LFD) solver. It allows to identify the linear response of the flow to an oscillating variation of a boundary condition, e.g. a deflecting control surface, for a single frequency. The shape of the motion and the direction of the oscillatory movement is thereby incorporated in the response. By superposition of the responses of multiple frequencies according to a Fourier transformation, the aerodynamics response for an arbitrary control surface deflection profile

☆ This article is part of a Special issue entitled: 'AERO2025' published in International Journal of Heat and Fluid Flow.

* Corresponding author.
E-mail addresses: ruben.seidler@dlr.de (R.B. Seidler), reingard.geisler@dlr.de (R. Geisler), andreas.schroeder@dlr.de (A. Schröder), jochen.wild@dlr.de (J. Wild).

https://doi.org/10.1016/j.ijheatfluidflow.2025.110177
Received 17 July 2025; Received in revised form 12 November 2025; Accepted 2 December 2025
Available online 5 December 2025

may be computed and predicted in real-time (Seidler et al., 2020a). For verification of the numerical simulations, unsteady simulations using the LFD solver and URANS equations were performed. Previous works on the application of LFD results for control surface deflections (Seidler et al., 2020a) and gust loads (Seidler et al., 2020b) have proven the viability of this method for the accurate and efficient prediction of the aerodynamic responses. Once the LFD solver has computed the surface pressure response for a sufficient range of frequencies, the total unsteady response in lift or drag due to an arbitrary change in control surface angle or gust speed can be predicted within milliseconds for this flight condition. Using the result from the LFD solver in a surrogate model enables this prediction speed for all covered flight conditions and geometric shapes, given that the response remains in a linear flow region. The studies also showed, that LFD and URANS simulations lead to the same result, as long as the control surface has small deflections amplitudes and no strong nonlinear effects such as shocks or flow separation are formed during the deflection. A first validation of the LFD solver was conducted on the DLR-F12 full aircraft model (Widhalm et al., 2012), which featured a reduced frequency of $k = 0.0646$ and remained in the quasi-steady aerodynamic region. In this study, for the validation of the results of the LFD solver in the unsteady flow region, a wind tunnel experiment was conducted. The wind tunnel experiment was especially designed to validate the prediction quality and the validity range of the LFD simulations. Therefore, an extension to a 2D airfoil model was designed, that consists of a control surface, which is accurately controlled and can achieve high accelerations of its deflection angle in both directions. Thereby sinusoidal oscillations and arbitrary movement profiles of the control surface with sudden changes in velocity are feasible. The usage of a linear electric servo motor with fast acceleration and the implementation of unsteady pressure sensors on the wing allowed the generation and measurement of the unsteady aerodynamic flow field around an airfoil with a fast acting control surface. An important parameter for the description of unsteady aerodynamics is the reduced frequency k:

$$k = \frac{2\pi f l_{\text{ref}}}{2v_\infty}$$

In this equation l_{ref} is a chosen reference length (here the chord length c), f is the oscillation frequency and v_∞ is the flow velocity. Reduced frequencies of 0.05 and higher are considered as unsteady, whereas reduced frequency of over 0.2 describe highly unsteady aerodynamics (Sears, 1941).

2. Wind tunnel experiment

The wind tunnel model for the experiment is the DLR-F15 airfoil model (Wild, 2013), which is an extruded 2D-airfoil with a chord length of 0.6 m and a span of 2.8 m, extending between two wind tunnel walls. The model has been used to investigate the effect of different high-lift system devices and has exchangeable parts for its slat and flap. Recently the model has been extended by a deflecting spoiler (Geisbauer, 2021). For the wind tunnel experiment the rear part of the flap was replaced by a small controllable control surface, which is called the flap-tab (Dargel et al., 2002). In Fig. 1 the wind tunnel model with the flap, spoiler and flap-tab (deflected by $-30°$) is shown. The flap-tab thereby has the same spanwise width as the spoiler of 0.6 m. The flap-tab replaces the spanwise middle part of the flap trailing edge, whereas the flap has a chord length of 28% airfoil chord and the flap-tab has about 11% airfoil chord. On the bottom-right of the 3D view, the drive shafts of the spoiler and the flap-tab can be seen. In this experiment the flap-tab was dynamically deflected and the spoiler was set to a fixed position. The flap-tab is designed that it can be deflected by 30° in upward and downward direction even when flap and spoiler are retracted. A positive deflection represents a downward deflection. The drive shaft of the flap-tab is actuated by a servo motor, which enables to reach an acceleration of up to $10,000°/s^2$ on the flap-tab in both directions. For an excitation of the flap-tab of 30° the flap-tab can reach a deflection rate of $775°/s$ and for a sinusoidal oscillation with 5° amplitude the flap-tab can be oscillated with a frequency of 6 Hz. For the lowest Mach number of 0.1, reduced frequencies of 0.645 can be achieved in the experiment. A further increase of the reduced frequency would theoretically be possible by reducing the Mach number of the wind tunnel flow even further. Nevertheless, this would lead to relatively low-pressure changes at the limits of sensitivity range for the applied measurement techniques, mainly the chosen range of pressure scanners for local surface pressure measurements. Therefore, lowering the wind tunnel flow speed even further was not pursued.

2.1. Setup in the low-speed wind tunnel

The wind tunnel in use is the low-speed wind tunnel in Braunschweig called the Niedergeschwindigkeits-Windkanal Braunschweig (DNW-NWB), which was setup with its closed-loop test section. The DLR-F15 wind tunnel model thereby was positioned vertically, so that its left and right end were flush with the top and bottom wall. The wind tunnel has a height of 2.8 m and a width of 3.25 m. The wind tunnel is able to reach Mach numbers of 0.25 and for the DLR-F15 model Reynolds numbers of up to $3 \cdot 10^6$ were reached. Due to geometrical constraints resulting from camera positions of the measurement setup, the angle of attack was at a fixed position. Therefore, only results using the angle of attack of $\alpha = 0°$ are presented. Preliminary studies showed, that the flow was attached over the airfoil for this setting and most of the unsteady effects due to the flap-tab deflection were invariant to small changes in the angle of attack. The time-resolved deflection angle of the flap-tab was recorded in two ways. First, an internal angular sensor was implemented directly at the flap-tab, and second, an optical, so called picColor measurement system was applied. For the latter, the luminescent yellow markers shown in Fig. 2 are tracked by a stereo camera system. The picColor System can track the flap-tab angle with a caption rate of 800 Hz and serves as the main source for the measurement of the deflection angle. The angular internal sensor indicates the angle in $0.9°$ angle steps due to binary resolution, which served as a backup for accuracy measurements. For the accurate measurement of the unsteady aerodynamics on the wing surface 42 unsteady pressure transducers were distributed along the middle section of the wing. They had a caption rate of 800 Hz and were used as the main source for pressure measurements on the wing. The wing also featured a high number of classical static pressure probe drillings on the wing. Due to the long tube length they have a too high damping for capturing the unsteady aerodynamics and thus are regarded for static mean surface pressure measurements for the steady case. The pressure measured by the sensors is uncorrected, since the effect of the wind tunnel due to its size is negligible and the corrections are not made for unsteady measurements. In addition to the pressure transducer measurement in the wind tunnel, two further measurement techniques were applied: Pressure Sensitive Paint (PSP) for the surface near the flap-tab and Particle Image Velocimetry (PIV) for the measurement of the field flow. The PSP measurements however were in an early development status for the observation of the relatively low surface pressure variation levels by high-frequency detection cameras. Therefore, the subsequent extensive evaluation of the PSP tests showed high discrepancies in the data and made them unusable.

2.2. Flow-field measurement

The flow field around the DLR-F15 model with moving flap-tab has been observed dynamically by 2D-three components PIV in the middle section of the wing. The setup for PIV consists of a single laser light sheet and two cameras for each observed area, and a timing unit. On the suction side as well as in the wake of the wing the flow is observed with a field of view of about 200 mm × 200 mm each, shown in Fig. 3, where the calibration grid is attached to the wing at the observed section. The

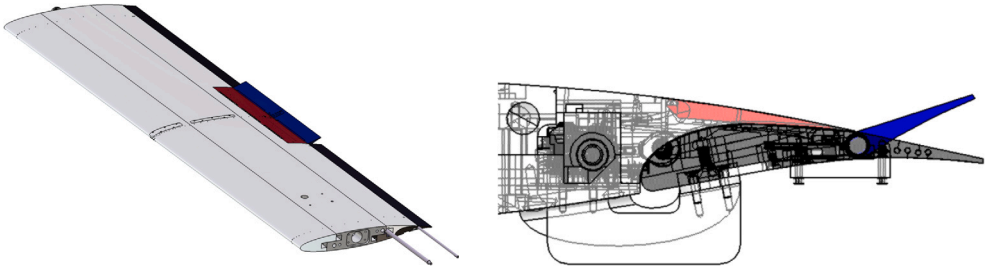

Fig. 1. DLR-F15 wind tunnel model with flap (black), spoiler (red) and flap-tab (blue). (For interpretation of the references to color in this figure legend, the reader is referred to the web version of this article.)

Fig. 2. Bottom view of the wing with luminescent circles on the flap-tab for the picColor-System. (For interpretation of the references to color in this figure legend, the reader is referred to the web version of this article.)

field of view on the suction side captures the flow in the middle of the suction side and upstream of the flap. The second field of view captures the flow around the moving flap-tab and in the near wake. Each field of view is imaged by two PCO.edge double-shutter cameras in stereo geometry from the top of the wind tunnel. Illumination of the fields of view is provided by a laser system consisting of two Quantel Big Sky Evergreen 200 dual-cavity pulse lasers combined to deliver a total energy of 400 mJ per illumination pulse. The combined laser beam is guided from the laser system to the side wall of the wind tunnel and formed to a horizontal light sheet by an arrangement of lenses. After reflection from a final adjustment mirror, the light sheet enters the test section through a slit in the wind tunnel side wall (Fig. 4) and illuminates both fields of view at the same time. The repetition rate of the acquisition is limited by the maximum laser (double-) pulse repetition rate of 15 Hz. This is fast enough to resolve 8 phases of 45° each in a 1 Hz flap oscillation, but in general it is too slow to cover all 8 phases within one cycle. Thus, for the flap oscillations above 1 Hz an interleaved acquisition was used to record 8 phases in 3 or 5 flap oscillation cycles. Each phase was thereby averaged over at least 3000 samples, so that a sufficient statistical accuracy over the velocity of the particles was reached. The acquisition sequence was triggered phase-locked from a cycle start signal provided by the flap actuation system. For each configuration the first phase position (45°) was manually adjusted with a programmable delay to fit the same geometric position. This was necessary to compensate the frequency- and amplitude-dependent electric and mechanic phase shift of the flap actuation. Due to the actuation of the flap-tab from the side the drive system incorporates a significant elasticity. Although the position was measured accurately by the picColor system, the drive control has to be adjusted to compensate for the stiffness internal to the actuation drive train. For the data evaluation an iterative multi-grid cross-correlation algorithm with image deformation was applied. The final interrogation window size was 20 × 20 pixels (1.67 mm × 1.67 mm) and the vector spacing 7 pixels (0.58 mm).

3. Numerical simulation setup

For the numerical simulations of the aerodynamics the Reynolds-averaged Navier–Stokes (RANS) equations were used, which were computed by the DLR-TAU solver (Gerhold, 2005). The turbulence model in use was the negative Spalart–Allmaras (SA-neg) (Spalart and Allmaras, 1992), since from previous experience it showed a sufficient accuracy and good robustness in the numerical simulation. For time-resolved unsteady simulations the unsteady RANS (URANS) methodology applying a dual time-stepping was used.

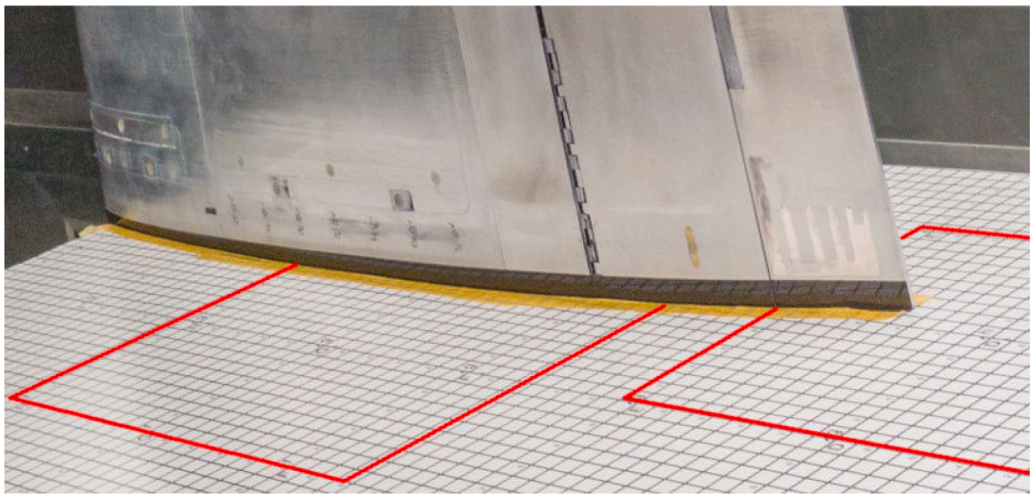

Fig. 3. A calibration grid is adjusted to the light sheet position for calibration of the cameras; the red lines in the picture indicate the approximate fields of view of the dual-stereo imaging system. (For interpretation of the references to color in this figure legend, the reader is referred to the web version of this article.)

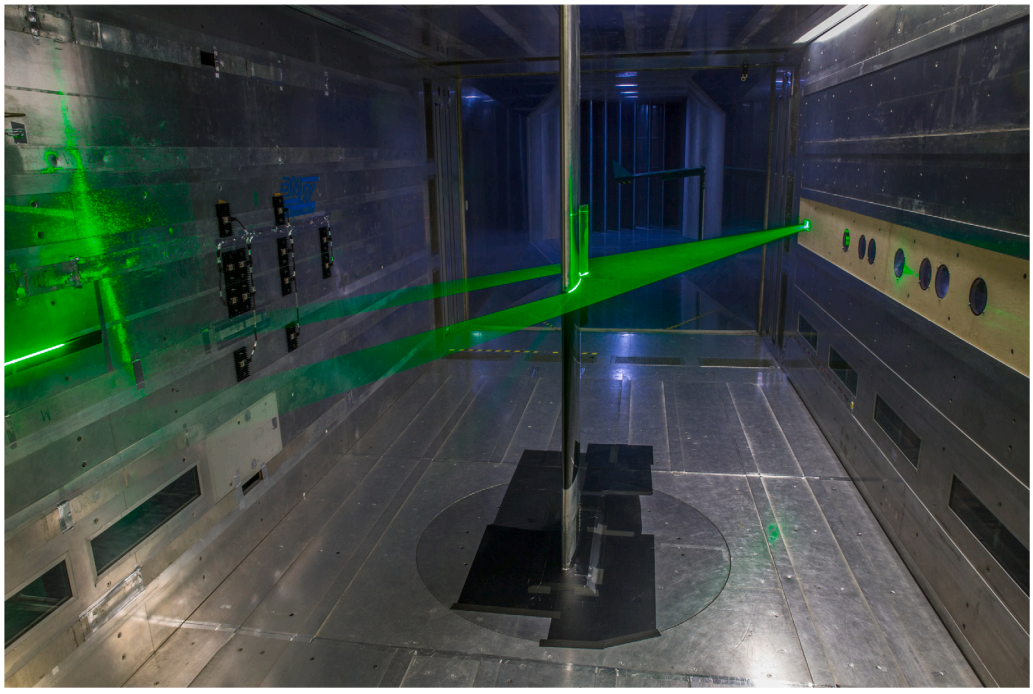

Fig. 4. The laser light sheet is emitted into the test section from downstream through a slit in the side wall.

3.1. Linear frequency domain solver

For the more efficient prediction of the unsteady aerodynamics of the flap-tab the DLR-TAU LFD solver was used in addition to the URANS simulations. The LFD solver computes a frequency response of the flow, which describes the reaction of the field state variables to an oscillation of any boundary condition, here the motion of a part of the geometry. The LFD solver always requires a steady RANS solution of its time-averaged mean and a predefined perturbation with a given frequency. Here, the perturbation is the movement of the grid points due to the flap-tab deflection angle δ_f and the LFD solver is run multiple times to predict the response to a wide frequency range for the oscillation of the flap-tab. The response of the local pressure in the flow field to the oscillating flap-tab is chosen as the output of the process. It is called the frequency response $\hat{g}$. The variable describes the response of the local pressure coefficient c_p for an oscillating flap-tab deflection angle δ_f for each circular frequency ω:

$$\hat{g}(\omega) = \frac{\partial c_p}{\partial \delta_f}(\omega) \tag{1}$$

Each value of frequency response $\hat{g}(\omega)$ is a complex number with a real and an imaginary part, with which a magnitude and phase shift can be calculated. The magnitude describes how much the local pressure coefficient changes for each change of the flap-tab deflection angle. The phase shift describes how much the responding c_p oscillation is behind or ahead of the δ_f oscillation. By integration of the local pressure on the surface the lift and pressure drag coefficient of the wing can also be computed. A full derivation of the equations of the LFD solver to compute the linear response of a RANS solution and further information on its functionality is given in Seidler et al. (2020a) and Thormann and Widhalm (2013).

Table 1
Description of the grid in use for each type of simulation, specified with its type of deformation and number of grid points.

Description	deform. type	num. of grid points
2D-LFD	RBF	≈483,000
2D-RANS	RBF	≈380,000
3D-LFD	RBF	≈33,289,000
3D-RANS	RBF/Chimera	≈35,563,000

3.2. Grid generation and deformation

The type of simulation demands for different kinds of grids for the simulation. For preliminary studies and the efficient simulation of the ideal characteristics of the moving flap-tab, a 2D grid with and without a gap was created. For the LFD solver the grid needs to be deformed in a way, that the total number of grid points remain the same. Therefore, a Radial-Basis function (RBF) deformation was used, which allows a smooth transition of the grid points. It can be seen exemplary for a small downward deflection for the 2D-grid with a gap between flap and flap-tab in Fig. 5. For the accurate simulation of the wind tunnel experiment three-dimensional grids were used to correctly model the effect of the limited span of the flap-tab. Although the full 3D simulation requires an order of magnitude more effort in grid generation and computational time, it was vital for the achieving an accurate simulation. Preliminary studies showed that the deflected flap-tab on the three-dimensional model had a strong difference in surface pressure to an equivalent two-dimensional model. The short spanwise width of the flap-tab of only 600 mm leads to a strong gradient in surface pressure in spanwise direction. The 3D grid was modeled using symmetry walls on each spanwise side of the wing and the airfoil was simulated under free-stream conditions between the two symmetry walls. For the LFD solver an additional 3D grid was created, which allowed the smooth deflection of the flap-tab for a small upward and downward angle. The URANS equations however require the possibility of a high deflection angle of the flap-tab and therefore the whole deflection needs to be modeled. Grid deformation alone would lead to extreme deformation or intersection of grid cells. Therefore, a Chimera or overset method was applied. For the modeling of the control surface deflection, the Chimera model consists of a block build around the flap-tab, in which the flap-tap is deflected by RBF deformation. The rigid mesh outside the block is connected to the deformed mesh inside the block over the walls of the block. For each new deflection angle, the grid points inside the block form new connections to the rigid mesh outside of the block. The block walls define an overlapping area, where the flow state is exchanged between the grids by interpolation. The grid of the Chimera model setup for the flap-tab can be seen in Fig. 6. In black the cells on the surface of the F15 model are shown, in blue the middle section cut of the boundary layer is shown, and in red the cells of the overlapping areas on the block walls are shown.

The Chimera model is not usable for the LFD solver, since in the Chimera method the grid points get blanked out due to changes of the overlapping region and thereby the number of cells for each deflection angle changes. It however is an established approach for URANS simulations of relatively moving bodies and thereby suitable for the flap-tab at high deflection angles. In Table 1 each kind of grid used for each simulation type is listed. The grid generation follows best practices as established in recent years. The number of grid points for each case are on the high end, up to the point where the computation time was still manageable for the preliminary tests and the reproduction of the wind tunnel tests.

4. Results

The wind tunnel data was evaluated and analyzed for each snapshot of the test series. Preliminary studies using numerical simulations were performed mainly on 2D grids using RANS and LFD solvers, in order to assess the scope of forces and moments on the flap-tab and get an understanding of its aerodynamic behavior. In order to assess the comparability of 2D studies to the wind tunnel experiment, a series of 2D simulations were performed in addition to their counterparts in 3D simulations of the wind tunnel experiment. Therefore, the surface pressure coefficient of a middle section cut of the 3D-RANS simulation was compared to a pure 2D-RANS simulation without a gap. The results can be seen in Fig. 7. It shows the surface pressure coefficient c_p over the wing geometry for four different deflection angles from 0° to 30° downward deflection. Although the 3D middle section cut has the same geometry as the geometry in the 2D simulation, the results in pressure coefficient differ distinctly. The influence of the flap-tab on the surface pressure is strongly decreased, especially at the leading edge of the wing. This shows, that for a direct comparison the wind tunnel experiment must only be compared to full 3D unsteady RANS and LFD simulations. Thus, for the most interesting cases, full 3D unsteady RANS simulations and a series of LFD simulations were performed and ultimately compared to the wind tunnel experiment. Since the different types of measurements lead to uncertainties in the time-accurate synchronization and in their absolute values, it was therefore necessary to apply accurate corrections to the simulated flap-tab deflection angle, so that always the real experimental process was simulated.

4.1. Comparison to RANS computation

In the first step, 3D RANS computations are compared to the wind tunnel data for static control surface deflections. The free-stream Mach number was set at 0.2 and the flap-tab oscillated with a frequency of 0.1 Hz between −10° and +7°. Fig. 8 shows the surface pressure coefficient for three distinct deflection angles of 0°, +7° and −10°. Overall the numerical simulations using a 3D grid are in good agreement with the wind tunnel data. The absolute values of c_p are captured well and they follow the same relative course for most of the wing geometry. Small discrepancies of about $\Delta c_p = 0.05$ can be seen mainly at the pressure side of the airfoil.

For visualization of the 3D-aerodynamics for a fast flap-tab deflection, a full 3D URANS simulation using the Chimera grid was made. For the shown case, a Mach number of 0.2 and a negative flap-tab deflection profile from 0° to −20° deflection angle was set. In Fig. 9 the simulated flow on the wind tunnel model is depicted, just at the time the flap-tab reaches the maximum negative deflection angle. The black lines show the streamlines over the flap-tab side gap. The background contour lines show the local Mach number in the wake at one chord behind the trailing edge and a cross cut in the middle section. Most notably is the occurrence of a strong vortex at the sides of the deflected flap-tab. This variation of the flow and the corresponding difference in surface pressure in spanwise direction explains the strong difference of the effectiveness of the flap-tab in 3D flow (either wind tunnel or simulation) to an ideal 2D simulation.

4.2. Visualization of flow field with PIV data

The analysis of the PIV velocity field data allows a deeper comparison of the flow state at two distinct areas of interest: the flow around the flap-tab and the flow on the upper surface of the wing upstream of the spoiler. As a first case for comparison, the flap-tab oscillating with a frequency of 1 Hz at an amplitude of 5°, a mean deflection angle of 0° and a Mach number of 0.1 is chosen, resulting in a reduced frequency of $k = 0.107$. In Fig. 10 the simulation of this case is shown, taken at a time instance, when the oscillating flap-tab reaches its minimum deflection angle of −5° and having the current speed of 0°/s. The value corresponding to the velocity magnitude of the white contour lines inside the two white marked areas are thereby the phase averaged data taken from the PIV measurements, the colored

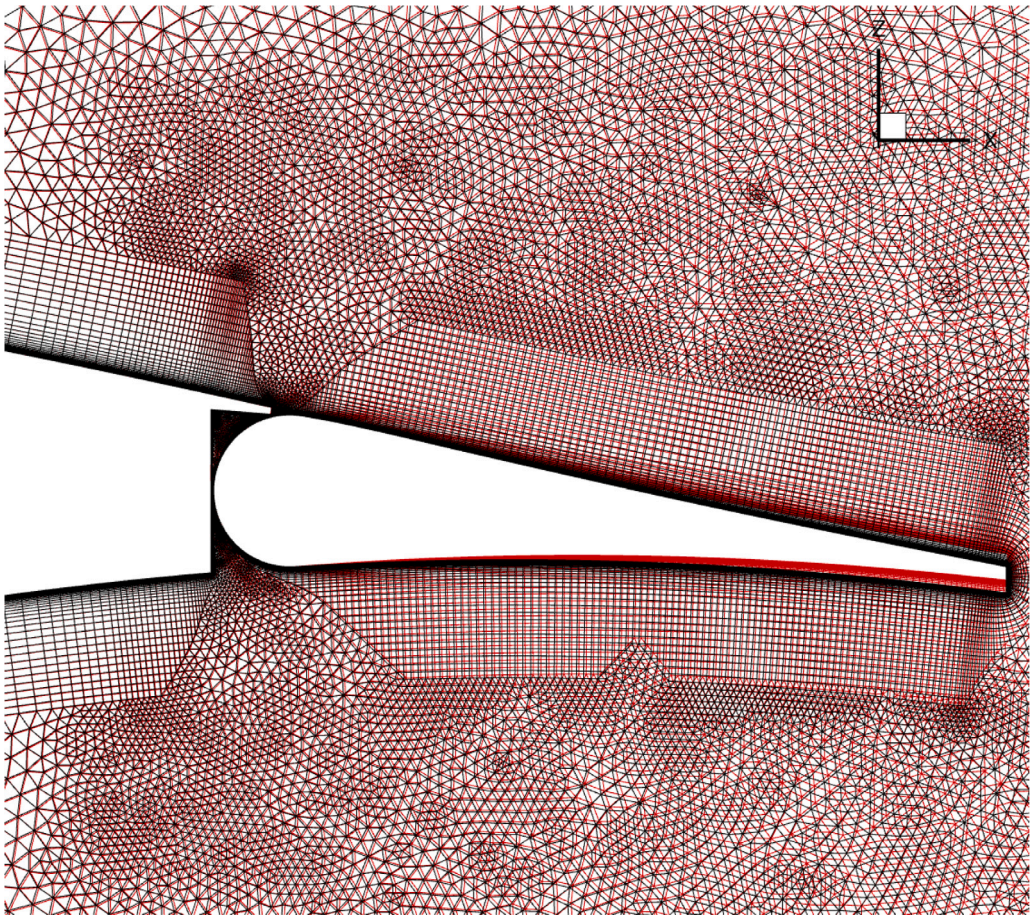

Fig. 5. Deformation of the 2D-grid with a gap between flap and flap-tab.

contour in the background is the velocity magnitude from the matching CFD simulation. The simulation shows a good agreement with the wind tunnel experiment. The overall behavior of the flow is matching and the pressure gradients near the flap-tab have the same shape at this phase. On the other hand, the absolute values are slightly different, with about $2\ \mathrm{m/s}$ more speed close to the surface on the upper side of the wing and $2-3\ \mathrm{m/s}$ less speed on the lower side of the flap-tab. These differences are not small, however, with the overall measurement accuracy of these highly unsteady effects and the simulation characteristics, these results undermine the valid usage of the simulation data for the assessment of loads and the analysis of the aerodynamics.

In Fig. 11 the case with the highest oscillation frequency for the flap-tab of 6 Hz is investigated. The amplitude is set at 5°, the mean deflection angle is 0° and the Mach number is set at 0.1, so that the highest reduced frequency possible in the experiment of $k = 0.646$ is reached. On the left side the evaluation of the wind tunnel aerodynamics using the PIV measurement is shown, whereas the right image shows the equivalent 3D-URANS simulation. The contour shows the local Mach number in the spanwise middle section of the wind tunnel model, where the results of the maximum and minimum deflection angle of ±5° in the oscillation are overlapped and shown, just in the moment these flap-tab angles were reached. The results of PIV and URANS data align, but still have deviations from each other. The PIV indicate lower Mach numbers in a narrow wake downstream of the flap-tab and less flow velocity downstream of the trailing edge from the maximum positive deflection angle. The URANS results show a broader wake, probably originating from a too coarse density of grid points in this area. Also, at about 0.75 m the overlapping boundaries of the Chimera grid technique are located, which might also cause small numerical errors on conservation over these boundaries. Nevertheless, for the higher oscillation frequency of 6 Hz, the relative behavior between the most upward and downward deflection is captured well and the PIV data fits the simulation data even in their absolute values. Still, this shows that the accurate simulation of unsteady aerodynamics requires a high number of grid points on and around the wing, due to the high vorticity and time-dependent fluctuations on and downstream of the moving control surface.

4.3. Comparison of dynamic pressure measurements to LFD results

For a direct comparison of the LFD results, the dynamics of the local surface pressure distribution on the wing are analyzed. Therefore, the measurements of the unsteady pressure sensors are compared to matching LFD computations. As an almost steady case, the oscillation with a low frequency of 0.5 Hz is chosen, whereas for a comparably unsteady case the highest oscillation frequency of 6 Hz is chosen. The Mach number is again set at 0.1, so that the highest reduced frequency occurs. In the experiment the flap-tab was actuated with a continuous time signal, so that an accurate sine curve was achieved. The accuracy of the 6 Hz flap-tab oscillation measurement can be seen in Fig. 12. Here, the magnitude of a fast Fourier transform (FFT) of the time signal of each Kulite and the flap-tap angle from the experiment is shown. The highest magnitude is reached at the target of 6 Hz, with two secondary peaks with one tenth of the value at 5.9 Hz and 6.1 Hz. Higher harmonics at 12 Hz and 18 Hz in the pressure response stay below an order of magnitude under the highest peak at 6 Hz. The target 6 Hz oscillation was therefore reached with a sufficient precision.

In Figs. 13 and 14 the comparison between LFD computation and wind tunnel experiment for these two frequencies are shown. The pressure measurements over time of the experiment were thereby

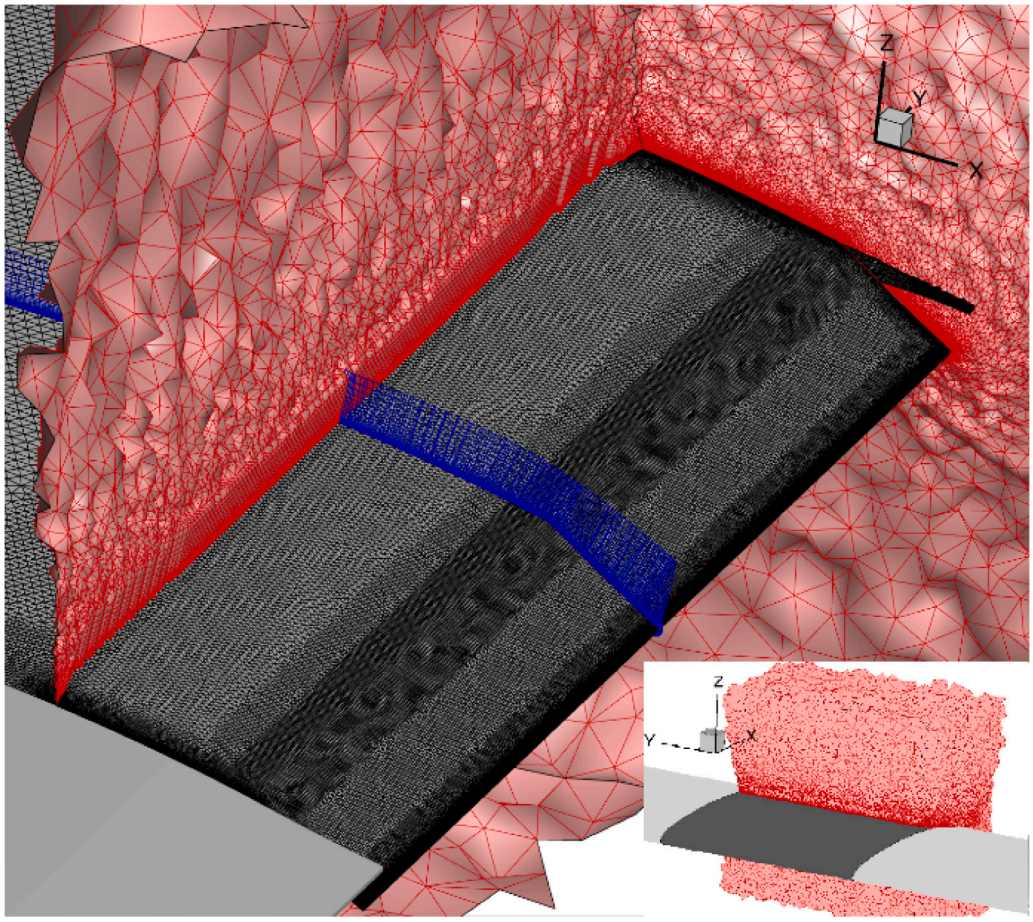

Fig. 6. Chimera-Setup for the flap-tab deflection in 3D with overlapping grid points on the chimera block walls (red) and the boundary layer grid structure (blue). (For interpretation of the references to color in this figure legend, the reader is referred to the web version of this article.)

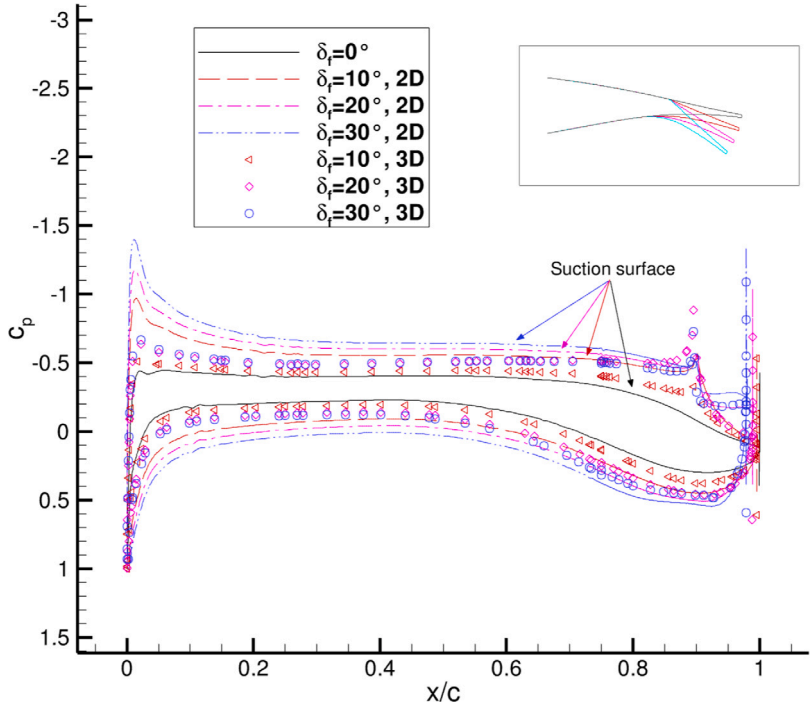

Fig. 7. Comparison of a 2D-simulation and the middle section of the 3D-wind tunnel model.

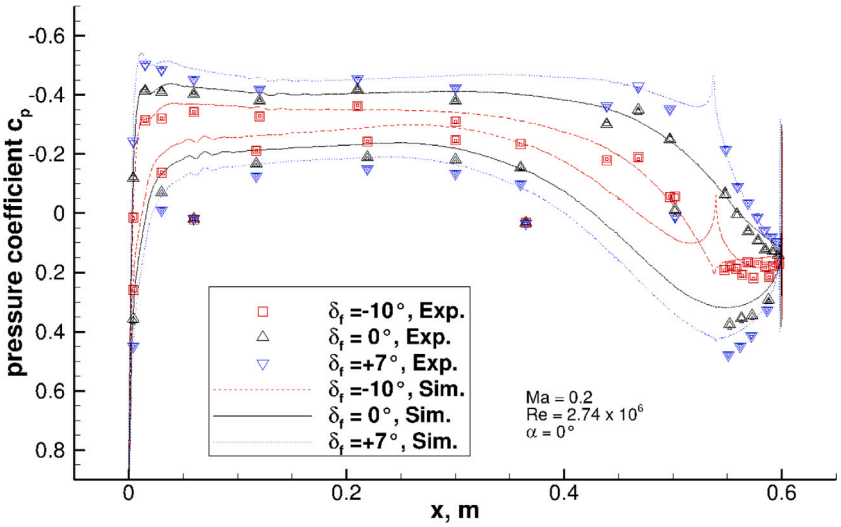

Fig. 8. Comparison between Experiment and Simulation for static deflections of 0°, +7° and −10° -results of three snapshots with different symbol sizes.

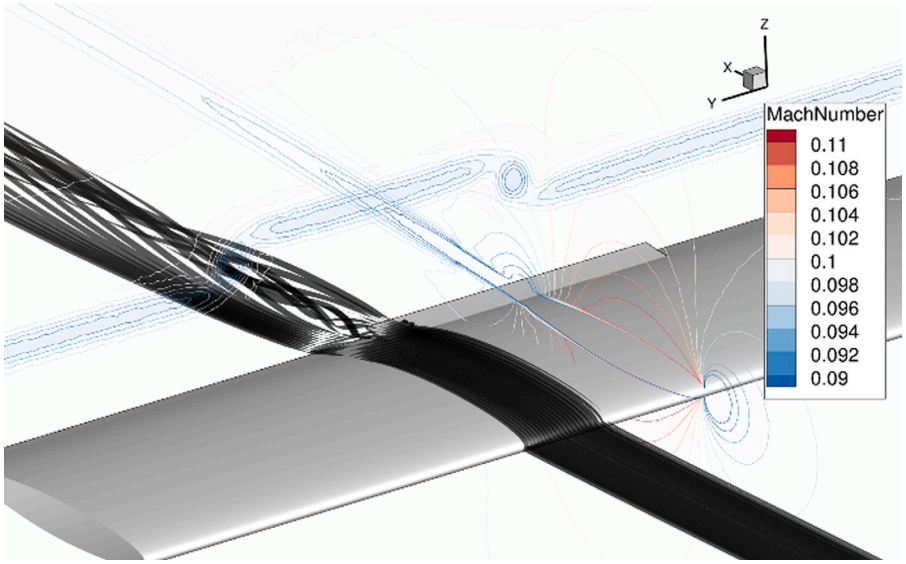

Fig. 9. Side edge vortices in the moment the flap-tab reaches −20°. Result of the fully unsteady 3D-simulation.

transformed into the frequency domain using a FFT. Fig. 13 shows the magnitude, which indicates the local change in pressure coefficient per flap-tab deflection angle c_p/δ_f for the oscillating flap-tab. We can see, that there is a good agreement between experiment and LFD simulation data. For both oscillations, the behavior over the airfoil is captured and the absolute values match well, near the leading edge and on the flap-tab. The results show, that the influence of the flap-tab on the leading edge pressure is lower for the higher frequency. The influence on the pressure near the flap-tab thereby is similar. This means that the smaller effectiveness in lift generation for the oscillation with 6 Hz is originated in the lower influence on the leading edge flow. The deflection of the flap-tab leads to a movement of the stagnation point due to a variation of the circulation. However, if the oscillation speed of the flap-tab is faster than the response of the stagnation point, the flow around the airfoil is not yet fully developed, when the maximum angle is reached. The time-dependent development of the pressure distribution on the leading edge then lags behind the one near the flap-tap. Therefore, for the frequency of 6 Hz, the lift generation using the flap-tab is lowered, which is captured very well by the LFD solver.

Fig. 14 shows the phase shift for this local surface pressure coefficient, which indicates the time shift of the surface pressure response related to the flap-tab oscillation. Here, also the experiment and LFD simulation data match very well. For the slow oscillation, the surface pressure coefficient has a small delay of up to 10° phase near the leading edge, while the faster oscillation has a negative 50° phase shift near the leading edge. The lag in phase shift increases the further the position is distant to the flap-tab. This indicates the time the pressure waves need to change the local pressure originated from the new flap-tab deflection angle. For the 0.5 Hz oscillation, the absolute time delay is 0.0555 s, while for the 6 Hz oscillation, it is 0.0231 s. This means, that the absolute response time is shorter for the higher oscillation frequency. The LFD solver matches well for the slow oscillation, while it indicates a constant offset by about −9° in phase shift compared to the experiment for the 6 Hz oscillation. This is equivalent to a constant 4 ms delay of the flap-tab angle signal of the experiment to an ideal signal in the simulation. Without this constant offset, the data between experiment and LFD solver match very well.

Also, the influence of the control surface deflection speed on the pressure distribution over the 3D-model is analyzed. In Fig. 15 the results from a 3D-LFD simulation for an oscillation with a Mach number of 0.1 and a reduced frequency of $k = 0$ and $k = 0.645$ are compared. Shown on the figure are the contour of the magnitude of the change of

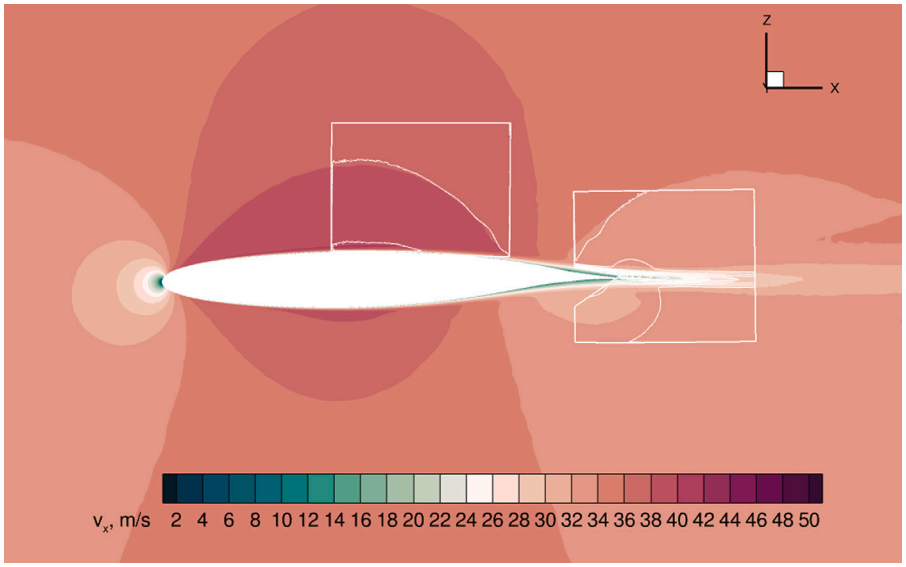

Fig. 10. Velocity field of the CFD-simulation (contour colors) and the evaluation of the PIV-results (white contour lines) in the PIV observation windows (white rectangles) for the flap-tab oscillating with 1 Hz at $M = 0.1$. (For interpretation of the references to color in this figure legend, the reader is referred to the web version of this article.)

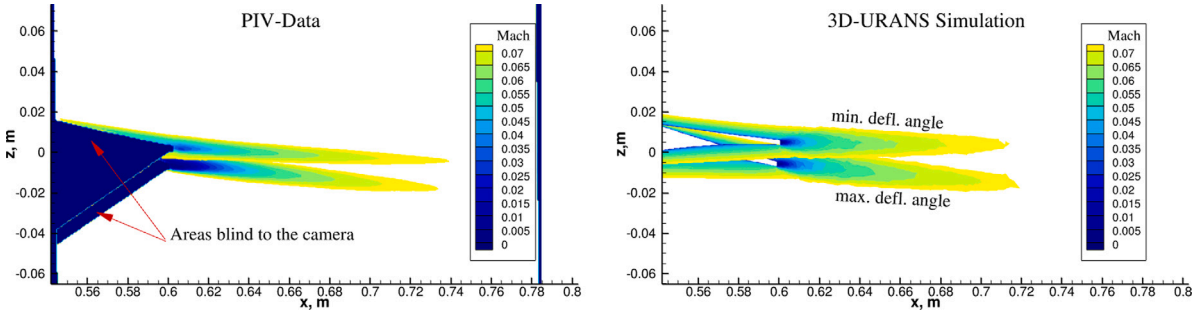

Fig. 11. PIV evaluation and 3D-URANS simulation for a 6 Hz oscillation of the flap-tab at M = 0.1. Shown are the Mach number of the wake in the middle-section for the minimum and maximum deflection angle.

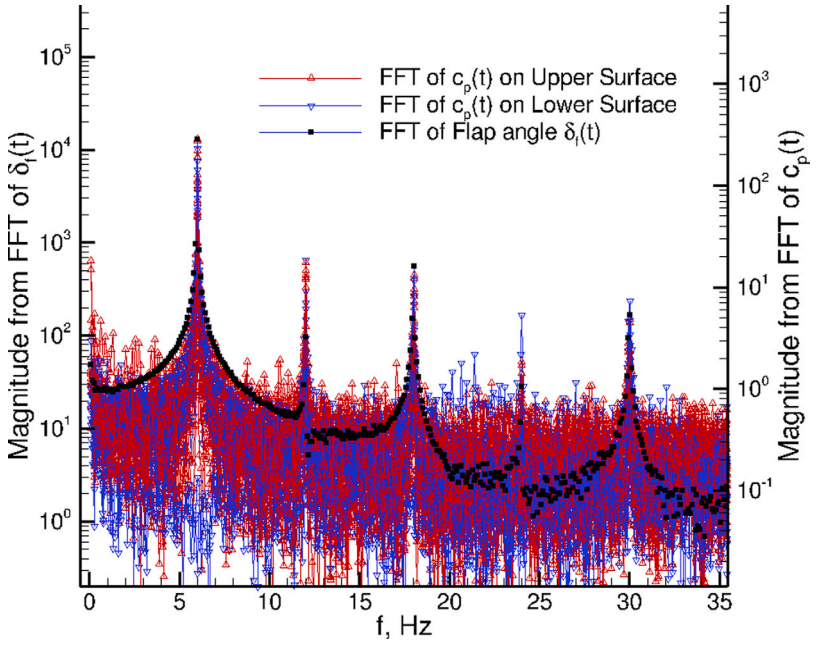

Fig. 12. Magnitude of a fast Fourier transform of each surface pressure coefficient and the picColor flap-tab angle due to the flap-tab oscillation for 6 Hz in the wind tunnel experiment. (For interpretation of the references to color in this figure legend, the reader is referred to the web version of this article.)

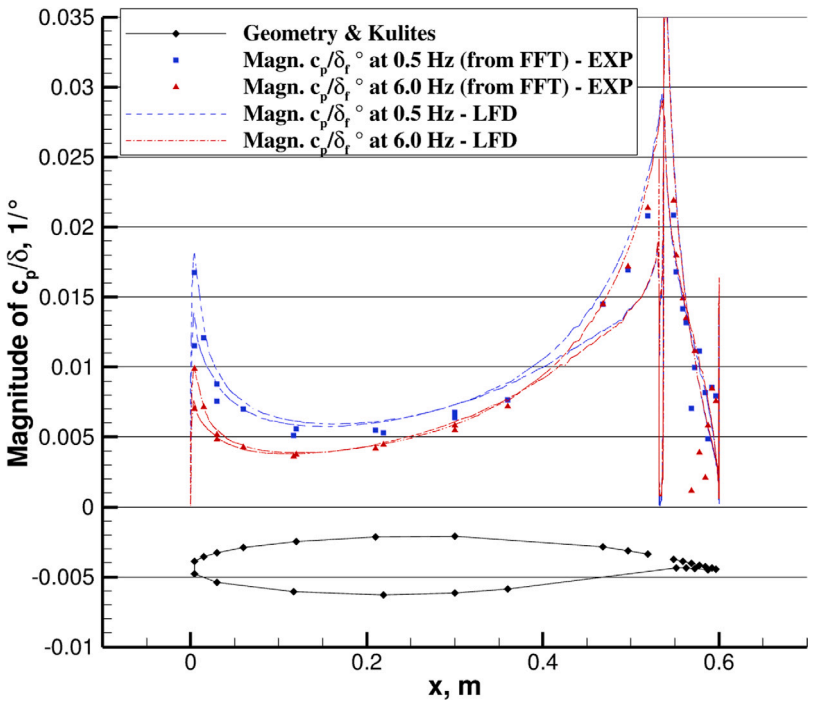

Fig. 13. Magnitude of the surface pressure coefficient due to the flap-tab oscillation with 0.5 and 6 Hz - comparison between wind tunnel experiment and 3D-LFD simulation.

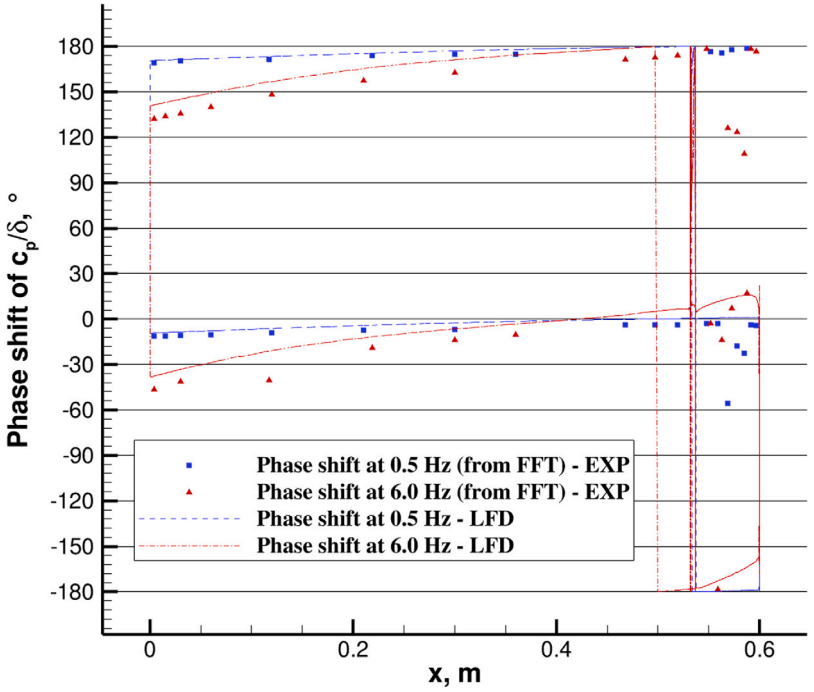

Fig. 14. Phase Shift of the surface pressure coefficient due to a flap-tab oscillation with 0.5 and 6 Hz - comparison between wind tunnel experiment and 3D-LFD simulation.

the surface pressure coefficient c_p to a change in the flap-tab deflection angle δ_f for each oscillation frequency k. A higher value thereby indicates, that the local pressure is strongly affected by the oscillating flap-tab. It can be seen, that, although the amplitude is the same, the oscillation frequency of the flap-tab, in other words its acceleration and speed, has a strong influence on the aerodynamics of the whole wing. As seen before in Fig. 14, the pressure coefficient on the leading edge for the reduced frequency of the $k = 0.645$ is much less affected by the flap-tab. The relocation of the stagnation point due to a new deflection angle takes too long to settle, before the flap-tab has already moved to a different position. Also, in spanwise direction we can see less influence of the flap-tab for the higher oscillation frequency. This shows, that for higher frequencies the flow physically further away from its geometric position is less affected.

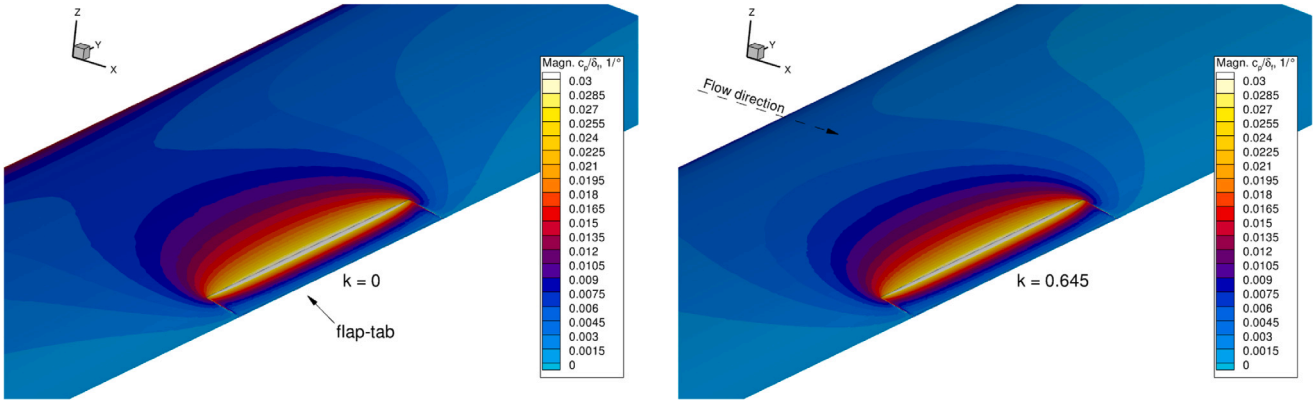

Fig. 15. Magnitude of $\hat{g}$ on the upper airfoil surface given by 3D-LFD simulations for two reduced frequencies of the flap-tab at M = 0.1.

5. Conclusion

In this work the results of an extensive study on unsteady aerodynamics of a fast-moving control surface using wind tunnel tests and numerical simulations are presented. The numerical simulations of the unsteady aerodynamics consisted of URANS simulations and a LFD solver, a tool suited for the efficient simulation of these unsteady responses in the frequency domain. The wind tunnel tests were used to validate the accuracy of these simulations, and to analyze and increase the understanding of the aerodynamic effects for fast moving control surfaces. The results show, that the simulations are well suited for the prediction of the aerodynamic responses on the wing. The LFD solver shows good agreement regarding the surface pressure with the wind tunnel test data, especially when considering the reduced setup time and the reusability of the frequency response data compared to fully 3D-URANS time-resolved simulations. Still, the accurate simulation of the unsteady aerodynamics, especially the full resolution of the gap flow and the vortices in the wake, require a high resolution in space and time. The studies show that increasing the oscillation frequency over $k = 0.1$ leads to the flow state having a time delay relative to the new control surface position and the response is not quasi-steady any more. The change in pressure due to the new control surface position needs time to fully adjust the position of the stagnation point near the leading edge. A phase shift between the change in pressure near leading and trailing edge occurs, which leads to the maximum local amplitudes in these two sections being out of sync. Also, the state of the flow is unable to fully develop for the maximum deflection angles with increasing oscillation frequency. These two effects lower the lift generation for reduced frequencies above the steady-state aerodynamics. In the 3D-simulations we can see that the influence on the pressure distribution for higher oscillation frequencies diminishes the further away it is located from the control surface. Especially the influence on the spanwise pressure distribution decreases for higher reduced frequencies. In the future it is important to increase the potential highest reduced frequency in the wind tunnel tests, in order to validate the methods for effects of even higher unsteady aerodynamics.

CRediT authorship contribution statement

Ruben B. Seidler: Writing – original draft, Visualization, Validation, Software, Resources, Project administration, Methodology, Investigation, Formal analysis, Data curation, Conceptualization. **Reinhard Geisler:** Writing – original draft, Visualization, Supervision, Software, Resources, Methodology, Data curation. **Andreas Schröder:** Writing – review & editing, Supervision, Resources, Project administration, Funding acquisition, Data curation. **Jochen Wild:** Writing – review & editing, Supervision, Resources, Project administration, Conceptualization.

Declaration of competing interest

The authors declare that they have no known competing financial interests or personal relationships that could have appeared to influence the work reported in this paper.

Data availability

Data will be made available on request.

References

Dargel, G., Hansen, H., Wild, J., Streit, T., Rosemann, H., 2002. Aerodynamische Flügelauslegung Mit Multifunktionalen Steuerflächen. DGLR-2002-096, Band I, p. 1605ff.

Geisbauer, S., 2021. Numerical simulation and validation of aerodynamics of static and dynamic spoilers. J. Aircr. 58 (6), 1187–1203. http://dx.doi.org/10.2514/1.C036145.

Gerhold, T., 2005. Overview of the hybrid RANS code TAU. In: MEGAFLOW - Numerical Flow Simulation for Aircraft Design. Springer Berlin Heidelberg, pp. 81–92.

Ghoreyshi, M., Jirasek, A., Cummings, R., Tomaro, R., Wurtzler, K., 2013. Static and dynamic loads modeling of an aerodynamic control surface. In: 51st AIAA Aerospace Sciences Meeting Including the New Horizons Forum and Aerospace Exposition 2013. http://dx.doi.org/10.2514/6.2013-664.

Giesseler, H.-G., Kopf, M., Varutti, P., Faulwasser, T., Findeisen, R., 2012. Model predictive control for gust load alleviation. IFAC Proc. Vol. 27–32.

Handojo, V., Himisch, J., Bramsiepe, K., Krüger, W.R., Tichy, L., 2022. Potential estimation of load alleviation and future technologies in reducing aircraft structural mass. Aerospace 9, http://dx.doi.org/10.3390/aerospace9080412.

Khalil, A., Fezans, N., 2021. Gust load alleviation for flexible aircraft using discrete-time H_∞ preview control. Aeronaut. J. 125 (1284), 341–364. http://dx.doi.org/10.1017/aer.2020.85.

Sears, W.R., 1941. Some aspects of non-stationary airfoil theory and its practical application. J. Aeronaut. Sci. 8 (3), 104–108. http://dx.doi.org/10.2514/8.10655.

Seidler, R.B., Marten, S., Widhalm, M., Wild, J., 2020a. Efficient prediction of aerodynamic control surface responses using the linear frequency domain. AIAA J. 58 (5), 1964–1975. http://dx.doi.org/10.2514/1.J058840.

Seidler, R.B., Widhalm, M., Wild, J., 2020b. Load control for unsteady gusts with control surfaces using the linear frequency domain. In: AIAA Aviation 2020 Forum. http://dx.doi.org/10.2514/6.2020-2670.

Spalart, P., Allmaras, S., 1992. A one-equation turbulence model for aerodynamic flows. In: 30th Aerospace Sciences Meeting and Exhibit. AIAA 1992-0439, http://dx.doi.org/10.2514/6.1992-439.

Thormann, R., Widhalm, M., 2013. Linear frequency domain prediction of dynamic response data for viscous transonic flows. AIAA J. 51 (11), 2540–2557. http://dx.doi.org/10.2514/1.J051896.

Vuillemin, P., Martin, D.Q., Poussot-Vassal, Ch., 2021. Performance evaluation of gust load alleviation systems for flexible aircraft via optimal control. Syst. Control http://dx.doi.org/10.48550/ARXIV.2107.00266.

Widhalm, M., Hübner, A.R., Thormann, R., 2012. Linear frequency domain predictions of dynamic derivatives for the DLR F12 wind tunnel model. In: ECCOMAS 2012. Vienna, Austria.

Wild, J., 2013. Mach and Reynolds number dependencies of the stall behavior of high-lift wing sections. J. Aircr. 50 (4), 1202–1216. http://dx.doi.org/10.2514/1.C032138.

Xu, J., Kroo, I., 2014. Aircraft design with active load alleviation and natural laminar flow. J. Aircr. 51 (5), 1532–1545. http://dx.doi.org/10.2514/1.C032402.